Received 20 December 2021; revised 18 January 2022; accepted 23 January 2022. Date of publication 26 January 2022; date of current version 22 February 2022.
The review of this article was arranged by Editor C.-M. Zetterling.

Digital Object Identifier 10.1109/JEDS.2022.3146368

Comparison of Short-Circuit Safe Operating Areas Between the Conventional Field-Stop IGBT and the Superjunction Field-Stop IGBT

ZHIHAO WANG, ZHI LIN (Member, IEEE), WEI ZENG, SHENGDONG HU (Member, IEEE), AND JIANLIN ZHOU

Chongqing Engineering Laboratory of High-Performance Integrated Circuits, School of Microelectronics and Communication Engineering, Chongqing University, Chongqing 400044, China

CORRESPONDING AUTHOR: Z. Lin (e-mail: linzhi@cqu.edu.cn)

This work was supported by the National Natural Science Foundation of China under Grant 62074020.

ABSTRACT This paper studies the short-circuit safe operating area (SCSOA) of the conventional field-stop (FS) IGBT and the superjunction (SJ) FS IGBT, based on 1200 V-rated samples, with the help of numerical electrothermal simulations. The results show that the peak electric field influences the distribution of the temperature inside devices and plays a crucial role in determining their SCSOAs. When the doping concentration of the collector, N_C, is low, the peak electric field exits near the collector. Both types of IGBTs have a long short-circuit time, T_{SC}, which can exceed 15 μs. T_{SC} decreases with the increase of N_C because the peak electric field transfers to near the channel. The introduction of the SJ structure weakens the peak electric field and increases T_{SC}. The difference is at least 4 μs and up to 6.87 μs, when N_C ranges from 2.0×10^{17} cm^{-3} to 1.1×10^{18} cm^{-3}. Besides, T_{SC} of the SJ IGBT can be increased by using highly-doped pillars.

INDEX TERMS Superjunction (SJ), field-stop (FS), short-circuit safe operating area (SCSOA), insulated gate bipolar transistor (IGBT).

I. INTRODUCTION

The insulated gate bipolar transistor (IGBT) has been widely used in power electronics, especially in medium and high power equipments [1]. It combines the advantages of fast switching, low conduction loss, and high impedance gate control. The basic concern of IGBTs is the trade-off relationship between the on-state voltage, V_{on}, and the turn-off loss, E_{off}. To improve this trade-off, new device structures are constantly being proposed, from the punch-through (PT) IGBT [2] and the non-punch-through (NPT) IGBT [3] to the field-stop (FS) IGBT [4]. To further improve the relationship, the superjunction (SJ) FS IGBT was proposed [5]. The superjunction structure in the drift region leads to a significant reduction in V_{on} and E_{off} [6].

While improving the trade-off relationship, other characteristics, such as the short-circuit safe operating area, should not be adversely affected. The short-circuit safe operating area (SCSOA) is an important parameter in applications because the short-circuit switching is one of the most severe stress conditions on IGBTs [7]–[8]. There are two kinds of short-circuit destruction which are electrical destruction and energy destruction respectively [9]. Electrical destruction is caused by current filaments which appear when the impact ionization in the anode side exceeds a critical avalanche generation rate [10]. Inside the current filament, the higher electron current density induces larger impact ionization in the n-drift/n-buffer junction, resulting in higher collector current peak [11]. Energy destruction is also named thermal destruction, caused by thermal runaway. In a short-circuit condition, the device supports the entire external voltage while conducts a large current. It consumes a high power and its temperature rises sharply. If this situation persists, thermal runaway will happen and the device will be permanently destroyed at last. Therefore, the device should be switched off in time to keep it safe. The time duration over which the IGBT structure can withstand the short-circuit

This work is licensed under a Creative Commons Attribution 4.0 License. For more information, see https://creativecommons.org/licenses/by/4.0/

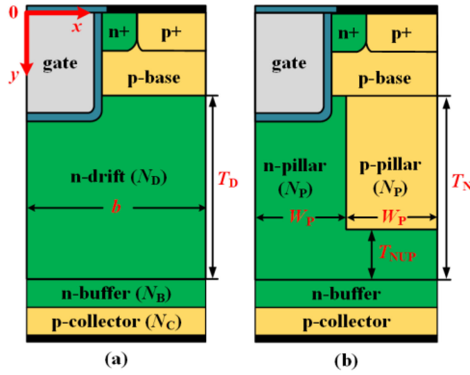

FIGURE 1. Schematic half-cell cross-sections of the (a) conventional and (b) SJ FS IGBTs, both with a trench gate. The difference is the drift region.

condition is defined as short-circuit time, T_{SC}, the longer, the better. In general, 10 μs is required [12]. This paper aims to study the energy destruction of the conventional and the SJ IGBTs.

Although previous studies have shown that the introduction of the superjunction structure [13] will not reduce T_{SC} of FS IGBTs, there is currently no special study to discuss this issue. In this paper, we compare the SCSOA between the conventional FS IGBT and the SJ FS IGBT, based on 1200V-rated samples, with the help of numerical electrothermal simulations. Based on theoretical analysis and simulation results, we find that the peak electric field influences the distribution of the temperature inside devices and plays a crucial role in determining their SCSOAs. The introduction of the SJ structure weakens the peak electric field and increases T_{SC}. Besides, influences of the doping concentration of the collector and the doping concentration of the drift region on T_{SC} are also discussed.

II. STRUCTURE AND THEORETIC ANALYSIS

Fig. 1(a) and (b) show structures of the conventional field-stop (FS) IGBT and the superjunction (SJ) FS IGBT, respectively. Compared with the conventional FS IGBT, the drift region of the SJ FS IGBT is replaced by alternative n-type and p-type pillars. Both structures feature the same MOS gate dimensions. The width and depth of the trench are respective 1.5 μm and 2.5 μm. The thickness of the gate oxide is 0.1 μm. Key parameters of 1200V-rated IGBTs are listed in Table 1. Their definitions are shown in Fig. 1. The numerical simulator Sentaurus Device [14] is used to explore the electrothermal performance of devices. The following models are active: Slotboom bandgap model, Shockley–Reed–Hall and Auger recombination models, the normal electric field dependence model, the carrier mobility model including high field saturation, and Philips unified mobility model. The collector contact is set as the thermode with a thermal resistance of 0.3 K/W. Its initial temperature is 300 K. The gate and emitter contacts are set to be adiabatic. Furthermore, the default parameter file is used. The lifetime is 10 μs for electrons and 3 μs for holes.

TABLE 1. Key device parameters.

Parameters	Definitions	Values
b (μm)	half-cell width	4
N_D (cm^{-3})	n-drift concentration	1.0×10^{14}
W_P (μm)	n/p-pillar width	2
N_P (cm^{-3})	n/p-pillar concentration	4.0×10^{15}
T_D (μm)	n-drift thickness	95
T_N (μm)	n-pillar thickness	95
T_{NUP} (μm)	n-pillar thickness under p-pillar	5
N_B (cm^{-3})	peak n-buffer concentration	5.0×10^{16}
N_C (cm^{-3})	peak p-collector concentration	7.0×10^{16}-1.2×10^{18}

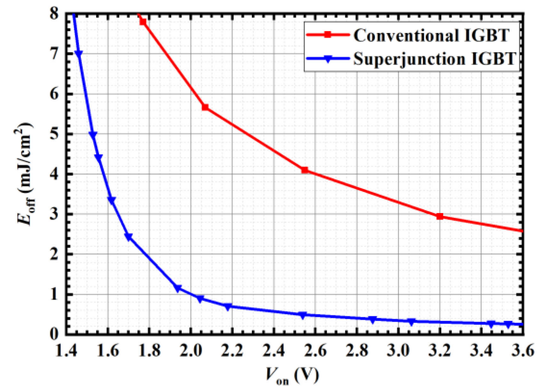

FIGURE 2. Trade-off relationship between E_{off} and V_{on} of IGBTs. N_D of the conventional IGBT is 1 × 10^{14} cm^{-3}. N_P of the SJ IGBT is 4 × 10^{15} cm^{-3}. N_C varies from 7.0 × 10^{16} to 1.2 × 10^{18} cm^{-3}.

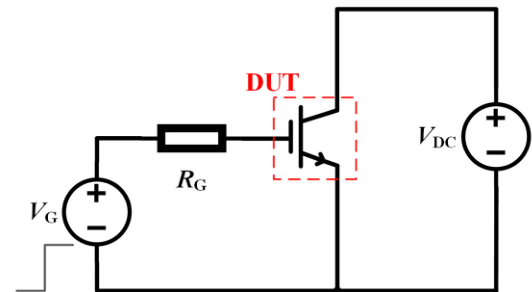

FIGURE 3. Circuit configuration for the short-circuit switching. V_{DC} = 600 V, R_G = 5 Ω. The active area of the device under test is 0.3 cm^2. The collector contact is set as the thermode with a thermal resistance of 0.3 K/W. Its initial temperature is 300 K.

First, switching characteristics of the two types of IGBTs are studied. Their switching current densities are all 100 A/cm^2. Trade-off relationship curves between E_{off} and V_{on} of IGBTs are shown in Fig. 2. Due to the impurity charge compensation effect, the doping concentration of the drift region of the SJ device can be an order of magnitude higher than that of the conventional one, which lowers the on-resistance and V_{on}. Then, the SJ IGBT has a better performance. Take $E_{off} = 3.4$ mJ/cm^2 for example, V_{on} of the SJ IGBT is 1.6 V, much smaller than that of the conventional one, which is around 3.0 V. Under this condition, V_{on} of the SJ IGBT is about 46.7% lower than that of the conventional one.

The short-circuit switching is analyzed by using the circuit shown in Fig. 3. The active area of the device under

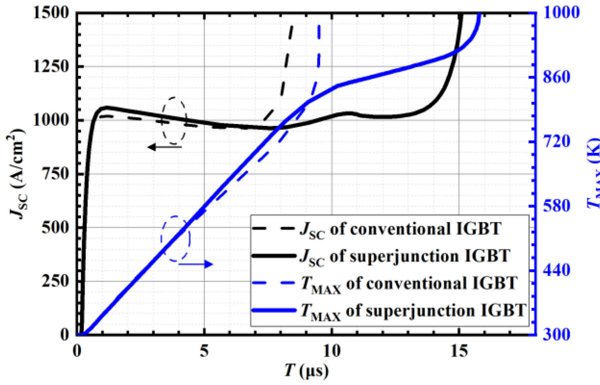

FIGURE 4. Changes of the short-circuit current density and the maximum temperature with time in an SJ IGBT (solid line) and a conventional IGBT (dashed line) with $N_C = 5 \times 10^{17}$ cm^{-3} under the short-circuit condition.

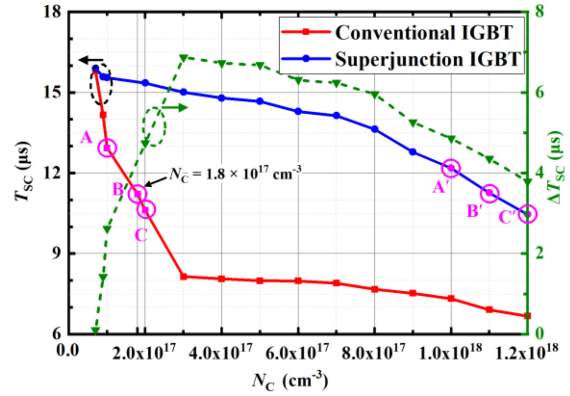

FIGURE 5. Extracted T_{SC} and ΔT_{SC} of IGBTs with different N_C. J_{SC} is set as 1000 A/cm^2 manually by adjusting the gate voltage.

test (DUT) is 0.3 cm^2. The dc-link voltage, V_{DC}, is set to be 600 V. A step signal is applied to the gate electrode of the DUT through a 5 Ω resistor. The short-circuit current density, J_{SC}, is 1000 A/cm^2. Fig. 4 shows SCSOA curves of the conventional IGBT and the SJ IGBT with $N_C = 5 \times 10^{17}$ cm^{-3}. After the DUT is completely switched on, its short-circuit current density drops slightly while its maximum temperature gradually increases from 300 K, over time. Thermal runaway happens at about 8 μs for conventional IGBT and 14 μs for SJ IGBT when the short-circuit current density rises sharply.

In the short-circuit condition, as shown in Fig. 3, the dc-link voltage is applied at the collector side while the device is switched on. Electrons are injected into the lightly-doped drift region from the n$^+$ emitter through the channel. Holes are injected from the p-collector into the drift region as well. They influence the effective doping concentration, N_{eff}, of the drift region, which can be expressed as

$$N_{\text{eff}} = N_D - n + p \tag{1}$$

where N_D, n and p are respectively, the concentration of donors, electrons and holes. Then, the expression of Poisson equation is now

$$\nabla \cdot \vec{E} = \frac{q}{\varepsilon_S} \cdot N_{\text{eff}} \tag{2}$$

where q and ε_S are respectively, the electron charge and the permittivity of silicon. They are constant. So, the electric field is determined by N_{eff}. For an IGBT with a buffer layer, electrons may be greater than the sum of donor impurities and holes, causing the electric field to be reversed in such conditions [15].

Since the DUT supports the entire external voltage while conducts a large current in the short-circuit condition, its power consumption is very huge. A large quantity of energy is dissipated in the form of Joule heat in a short time. As a result, the temperature of the device rises rapidly. On the micro-level, the temperature doesn't distribute uniformly inside the device. The density of Joule heat can be calculated as

$$\sigma = \overrightarrow{J} \cdot \overrightarrow{E} \tag{3}$$

Thus, heat generates more in the region with both a high current density and a high electric field. What we care about most is the temperature near the channel, because high temperature near the channel will reduce the built-in potential, V_{bi}, of the n$^+$-emitter/p-base junction. Finally, V_{bi} thermally disappears and the n$^+$-emitter/p-base junction is turned on. The short-circuit current will flow through the n$^+$-emitter/p-base junction now and not be controlled by the gate electrode anymore. Then, thermal runaway happens [16]. Therefore, the temperature near the channel has a greater impact on T_{SC}.

III. RESULTS AND DISCUSSION

A. THE INFLUENCE OF N_C ON T_{SC}

Fig. 5 shows the simulated T_{SC} of the two types of IGBTs with different N_C. The injection efficiency of the p-collector increases with the increase of N_C. The difference of T_{SC}, ΔT_{SC}, between these IGBTs is also shown. To avoid the influence of J_{SC} on ΔT_{SC}, J_{SC} is set as 1000 A/cm^2 for all samples by adjusting the gate voltage. When N_C is small, both conventional FS and SJ FS IGBTs show good capabilities of the SCSOA, with a long T_{SC}, which can exceed 15 μs. Besides, their T_{SC} both decrease with the increase of N_C.

There is still some difference between them. When N_C increases, the decline trends of T_{SC} of the two types of IGBTs show a clear difference. T_{SC} of the SJ IGBT decreases at a relatively stable rate. However, T_{SC} of the conventional one decreases sharply at first and then levels off. That is the reason why ΔT_{SC} increases first and decreases then as N_C increases. ΔT_{SC} reaches its maximum value of 6.87 μs when $N_C = 3.0 \times 10^{17}$cm^{-3}, after which T_{SC} of the conventional IGBT levels off. ΔT_{SC} also shrinks gradually after N_C is larger than 3.0 × 10^{17} cm^{-3}. In general, ΔT_{SC} between the two IGBTs is at least 4 μs and up to 6.87 μs, when N_C ranges from 2.0 × 10^{17} cm^{-3} to 1.1 × 10^{18} cm^{-3}.To explore the different performance of the two types of IGBTs in short-circuit conditions, several samples of T_{SC} curves

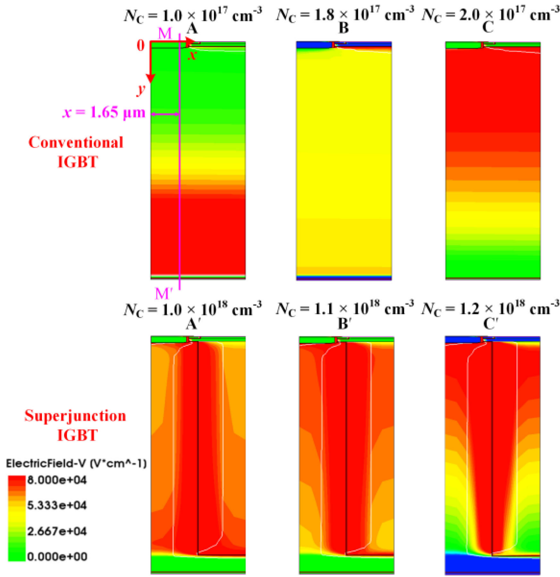

FIGURE 6. **Electric field distribution in IGBTs with difference N_C after shorted by 6 μs.**

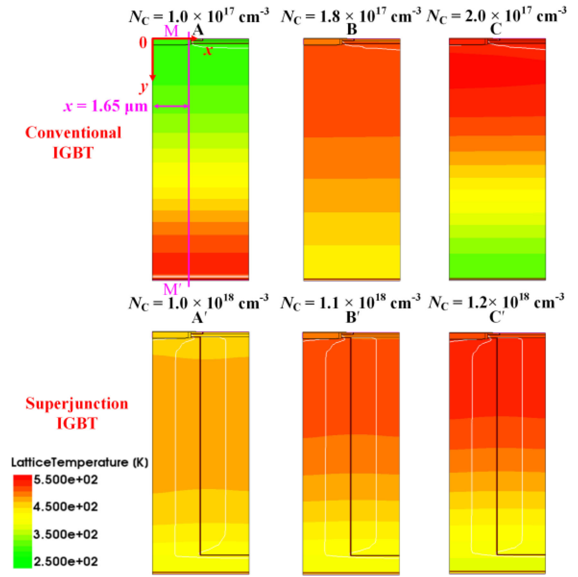

FIGURE 8. **Temperature distribution in IGBTs with difference N_C after shorted by 6 μs.**

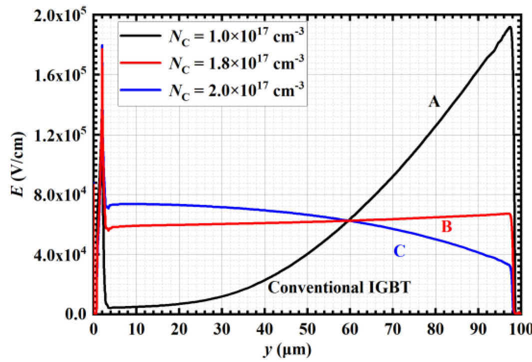

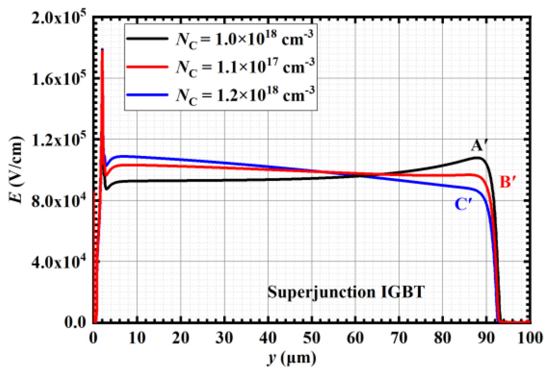

FIGURE 7. **Electric field distribution along y-direction at the cut-line MM′ ($x = 1.65$ μm) of Fig. 6.**

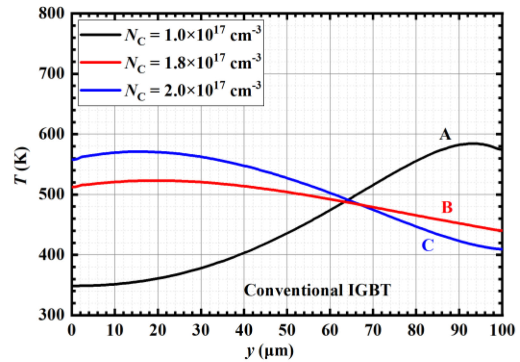

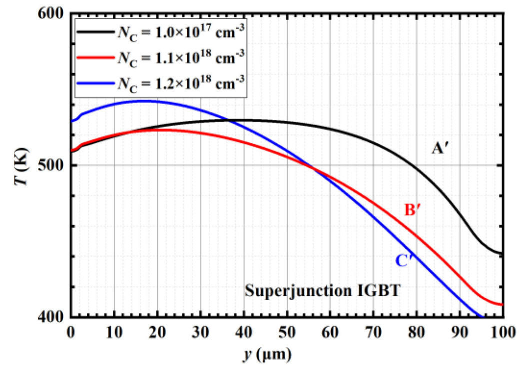

FIGURE 9. **Temperature distribution along y-direction at the cut-line MM′ ($x = 1.65$ μm) of Fig. 8.**

in Fig. 5 are picked and their internal states are analyzed. Their corresponding distributions of the electric field and temperature after shorted by 6 μs are shown in Fig. 6–9. As illustrated below, the position of the peak electric field changes in these samples, and so does the position of the maximum temperature. The electric field along the depth is almost flat in samples B and B'. Its slope is reversed around the sample B or B'. Take the conventional IGBT as an example. The slope of the electric field is reversed in the sample A, compared with that in the sample C. Thus, the

peak electric field appears near the collector in the sample A and the emitter in the sample C. For the conventional IGBT, samples A/B/C correspond to $N_C = 1.0 \times 10^{17}/1.8 \times 10^{17}/2.0 \times 10^{17}$ cm^{-3}. For the SJ IGBT, samples A'/B'/C' correspond to $N_C = 1.0 \times 10^{18}/1.1 \times 10^{18}/1.2 \times 10^{18}$ cm^{-3}. The results are analyzed as follows.

When N_C is small, the injection efficiency of the p-collector is low. Under this condition, the concentration of holes injected by the p-collector cannot exceed the doping concentration of the drift region when the current is conducting. Then, the concentration of electrons in the drift region is even greater than the sum of the concentration of donor impurities and the concentration of holes. N_{eff} in (1) is negative. So, the position of the peak electric field appears near the collector. Since the current density along the drift region is almost unchanged, the heating center is located at the bottom of the drift region. Then, the position of the maximum temperature appears near the collector. The channel temperature is relatively low. It needs a long time to reach the critical value that causes thermal runaway. As a result, T_{SC} is large.

The peak electric field changes with the changes of injected holes, causing a change in the temperature near the channel and a decrease in T_{SC}. As N_C increases, more holes are injected into the drift region and they can be injected deeper into the device. Holes slowly increase and electrons slowly decrease at the bottom of the drift region, causing the value of p minus n in (1) to grow. The negative N_{eff} decreases slowly. Then, the peak electric field decreases, and the electric field at the rest of the drift region increases slowly. Since the current density is maintained at 1000 A/cm^2 manually for different N_C, more heat is generated near the channel. Therefore, the channel temperature increases more at the same time. Thermal runaway happens earlier, resulting in a decrease in T_{SC}. This tendency continues until N_{eff} becomes positive.

$N_C = 1.8 \times 10^{17}$ cm^{-3} is the turning point of the conventional IGBT. At this time, N_{eff} in the drift region is almost zero. The electric field hardly changes along with the depth in the drift region. And, the electric field on the collector side is even slightly lower than that on the rest of the drift region. From now on, the electric field near the collector becomes lower than that near the emitter. The peak electric field and the heating center are now transferred to the channel region as well. Once N_C reaches 2.0×10^{17} cm^{-3}, conductivity modulation is nearly formed at the bottom of the drift region and the concentration of injected carriers becomes much higher than that of the drift region, resulting in a drastic decrease in T_{SC}. After that, N_{eff} hardly changes with the increase of N_C and so does the peak electric field. Increasing N_C only broadens the region with the conductance modulation effect. Therefore, T_{SC} of the conventional IGBT only slightly decreases with the increase of N_C, after N_C exceeds 3.0×10^{17} cm^{-3}. The difference is within 1 µs.

T_{SC} of the SJ IGBT is less affected by N_C because of the higher doping concentration of pillars, which is an order of magnitude larger than N_D of the conventional IGBT. Due to the high doping concentration of the pillars, holes injected into the pillars are far unable to form conductance modulation like the conventional IGBT when N_C increases to 2.0×10^{17} cm^{-3}. The turning point of N_C, which is corresponding to a flat electric field along with the depth, increases to 1.1×10^{18} cm^{-3}. For SJ IGBT, the concentration of injected carriers and the doping concentration of pillars are similar in magnitude. Therefore, when N_C increases, n and p just slowly change and the value of p minus n increases slowly as well, which further makes the change of the peak electric field slow. So it is for the temperature near the channel. Thus, T_{SC} of the SJ IGBT just decreases at a relatively steady and slow rate with the increase of N_C.

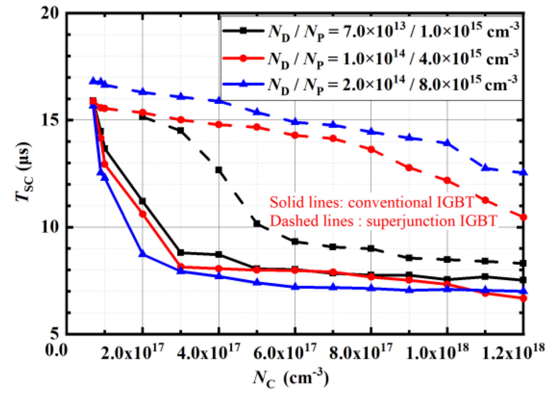

FIGURE 10. T_{SC} of three groups of IGBTs at J_{SC} = 1000 A/cm^2.

B. THE INFLUENCE OF N_D AND N_P ON T_{SC}

To find out the influence of N_D and N_P on T_{SC}, another two groups of IGBTs are simulated. Fig. 10 shows the simulated T_{SC} of these samples. Each group has the same breakdown voltage. There are no data for the SJ IGBT with $N_P = 1 \times 10^{15}$ cm^{-3} when its N_C is below 2.0×10^{17} cm^{-3}, because its saturation current densities are only a few hundred amperes per square centimeter. The simulation results are similar to those in part A. When N_C is small, both the conventional and the SJ IGBTs have a long T_{SC} because their peak electric fields are near the collector side. Their T_{SC} decrease with the increase of N_C, but at different rates.

What attracts attention is that T_{SC} of the SJ IGBT increases when the pillar concentration increases from 1.0×10^{15} cm^{-3} to 8.0×10^{15} cm^{-3}, while the change of N_D between 7.0×10^{13} cm^{-3} and 2.0×10^{14} cm^{-3} has almost no effect on T_{SC} of the conventional IGBT. For the conventional IGBTs with different N_C, their T_{SC} is almost the same under different N_D, because its N_D is much smaller than the concentration of injected carriers. As a result, N_D in (1) is almost negligible. The change of N_D has a very limited influence on the peak electric field and the temperature near the channel, causing T_{SC} to be almost unchanged. For SJ IGBTs with different N_P, there is a clear difference in their T_{SC}. In general, T_{SC} increases with the increase of N_P

when N_C is larger than 2.0×10^{17} cm^{-3}. As stated before, the doping concentration of pillars and the concentration of injected carriers are similar in magnitude. N_P plays a more important role in SJ IGBTs than N_D in conventional IGBTs. Since a bigger N_P introduces more lateral electric flux, the distribution of the electric field is flatter. Then, the peak electric field is reduced, resulting in a lower temperature near the channel under the same N_C.

It is noticeable that the turning point of the SJ IGBT with $N_P = 1.0 \times 10^{15}$ cm^{-3} is 4.0×10^{17} cm^{-3}. It is very close to those of the conventional ones which are 1.8×10^{17} cm^{-3}. Besides, the changing trend of the T_{SC} curve in Fig. 10 is similar to those curves of the conventional ones. That is because this N_P is comparable with N_D of the conventional ones, causing injected carriers to play a more important role in the change of T_{SC}. They all decrease sharply when N_C is around the turning point and then level off. Under this condition, ΔT_{SC} is above 4 μs only when N_C ranges from 2.0×10^{17} cm^{-3} to 4.0×10^{17} cm^{-3}. Therefore, on the premise that the breakdown voltage meets requirements, N_P of the SJ IGBT should be increased as much as possible to increase its T_{SC}.

IV. CONCLUSION

In the short-circuit condition, the IGBT supports the entire external voltage while conducts a large current. It consumes a high power and its temperature rises sharply. The temperature distribution in the device is determined by the distribution of the electric field, which is further determined by the concentration of injected carriers and the doping concentration of the drift region. And, the peak electric field plays a crucial role in determining SCSOAs of IGBTs. When the doping concentration of the p-collector, N_C, is small, both the conventional FS IGBT and the SJ FS IGBT have a long T_{SC}, which can exceed 15 μs. The reason is that the peak electric field and the maximum temperature appear near the collector. So, the channel temperature is low. As N_C increases, the peak electric field and the maximum temperature transfer to near the channel. Then, T_{SC} decreases. Since the doping concentration of the drift region of the conventional IGBT is relatively low, its peak electric field is more susceptible to the concentration of injected carriers. Its T_{SC} decreases sharply at first then levels off. And, its T_{SC} hardly changes when the doping concentration of its drift region changes from 7.0×10^{13} cm^{-3} to 2.0×10^{14} cm^{-3}. On the other hand, since the pillar concentration of the SJ IGBT is relatively high, its peak electric field is less susceptible to the concentration of injected carriers. Its T_{SC} decreases at a relatively stable rate with the increase of N_C. And, its T_{SC} increases when the pillar concentration increases from 1.0×10^{15} cm^{-3} to 8.0×10^{15} cm^{-3}. Besides, the SJ IGBT has a longer T_{SC} than the conventional IGBT with the same N_C.

REFERENCES

[1] N. Iwamuro and T. Laska, "IGBT history, state-of-the-art, and future prospects," *IEEE Trans. Electron Devices*, vol. 64, no. 3, pp. 741–752, Mar. 2017, doi: 10.1109/TED.2017.2654599.

[2] O. Saif and A. Hasan, "An extended model for a punch through (PT) trench insulated gate bipolar transistor (IGBT) and its transient characteristics," in *Proc. IEEE Region 10 Symp. (TENSYMP)*, Jun. 2020, pp. 427–430, doi: 10.1109/TENSYMP50017.2020.9231039.

[3] N. Patil, S. Menon, D. Das, and M. Pecht, "Anomaly detection of non punch through insulated gate bipolar transistors (IGBT) by robust covariance estimation techniques," in *Proc. 2nd Int. Conf. Rel. Safety Hazard Risk Based Technol. Phys. Failure Methods (ICRESH)*, 2010, pp. 68–72, doi: 10.1109/ICRESH.2010.5779635.

[4] L. Maresca *et al.*, "Temperature dependence of the on-state voltage drop in field-stop IGBTs," in *Proc. Int. Symp. Power Semicond. Devices ICs*, vol. 2018, Jun. 2018, pp. 144–147, doi: 10.1109/ISPSD.2018.8393623.

[5] F. Udrea, G. Deboy, and T. Fujihira, "Superjunction power devices, history, development, and future prospects," *IEEE Trans. Electron Devices*, vol. 64, no. 3, pp. 720–734, Mar. 2017, doi: 10.1109/TED.2017.2658344.

[6] M. Antoniou, N. Lophitis, F. Udrea, F. Bauer, U. R. Vemulapati, and U. Badstuebner, "On the investigation of the 'anode side' SuperJunction IGBT design concept," *IEEE Electron Device Lett.*, vol. 38, no. 8, pp. 1063–1066, Aug. 2017, doi: 10.1109/LED.2017.2718619.

[7] Y. Chen, W. Li, F. Iannuzzo, H. Luo, X. He, and F. Blaabjerg, "Investigation and classification of short-circuit failure modes based on three-dimensional safe operating area for high-power IGBT modules," *IEEE Trans. Power Electron.*, vol. 33, no. 2, pp. 1075–1086, Feb. 2018, doi: 10.1109/TPEL.2017.2682114.

[8] P. D. Reigosa, F. Iannuzzo, H. Luo, and F. Blaabjerg, "A short-circuit safe operation area identification criterion for SiC MOSFET power modules," *IEEE Trans. Ind. Appl.*, vol. 53, no. 3, pp. 2880–2887, May/Jun. 2017, doi: 10.1109/TIA.2016.2628895.

[9] R. Baburske, F.-J. Niedernostheide, H.-J. Schulze, R. Bhojani, J. Kowalsky, and J. Lutz, "Unified view on energy and electrical failure of the short-circuit operation of IGBTs," *Microelectron. Rel.*, vols. 88–90, pp. 236–241, Sep. 2018, doi: 10.1016/j.microrel.2018.06.091.

[10] M. Tanaka and A. Nakagawa, "Simulation studies for avalanche induced short-circuit current crowding of MOSFET-Mode IGBT," in *Proc. Int. Symp. Power Semicond. Devices ICs*, vol. 2015. Hong Kong, Jun. 2015, pp. 121–124, doi: 10.1109/ISPSD.2015.7123404.

[11] M. Tanaka and A. Nakagawa, "Simulation studies for short-circuit current crowding of MOSFET-Mode IGBT," in *Proc. Int. Symp. Power Semicond. Devices ICs*, 2014, pp. 119–122, doi: 10.1109/ISPSD.2014.6855990.

[12] B. J. Baliga, *Fundamentals of Power Semiconductor Devices*. New York, NY, USA: Springer, 2010.

[13] K. H. Oh *et al.*, "Experimental investigation of 650V super-junction IGBTs," in *Proc. Int. Symp. Power Semicond. Devices ICs*, vol. 2016. Prague, Czech Republic, Jul. 2016, pp. 299–302, doi: 10.1109/ISPSD.2016.7520837.

[14] *Sentaurus*^{TM} *StructureEditor User Guide*, Synopsys Inc., Mountain View, CA, USA, 2018.

[15] J. Lutz, H. Schlangenotto, U. Scheuermann, and R. De Doncker, *Semiconductor Power Devices: Physics, Characteristics, Reliability*. Heidelberg, Germany: Springer Int., 2018.

[16] M. Pfost, C. Unger, G. Cretu, M. Cenusa, K. Büyüktas, and U. Wahl, "Short-circuit safe operating area of superjunction MOSFETs," in *Proc. Int. Symp. Power Semicond. Devices ICs*, vol. 2016. Prague, Czech Republic, Jul. 2016, pp. 335–338, doi: 10.1109/ISPSD.2016.7520846.